Journal of Superconductivity and Novel Magnetism
https://doi.org/10.1007/s10948-021-06062-y

REVIEW

High-Temperature Superconductivity in Size-Selected Metal Nanoclusters: Gas-Phase Spectroscopy and Prototype Devices for Deposition Studies

Patrick J. Edwards[1] · Malak Khojasteh[1,2] · Avik Halder[1] · Vitaly V. Kresin[1]

Received: 9 September 2021 / Accepted: 9 October 2021

Abstract
Metal nanoclusters, composed of tens to thousands of atoms, display the phenomenon of electronic shell structure. This quantum size effect, with its associated level degeneracy, turns out to be highly propitious for superconductivity. Spectroscopy of free aluminum nanoclusters has revealed a pairing phase transition in their electron density of states at a temperature two orders of magnitude higher than the bulk. In addition to gas-phase research on this new family of high-T_c systems, it is important to pursue their use as building blocks for superconducting networks and assemblies. The development of devices suitable for the detection of superconductivity in surface-deposited nanoclusters is outlined.

Keywords Superconducting nanoparticles · Shell structure · Quantum size effect · Nanoclusters · Size-selective deposition · Carbon-based devices

1 Introduction

The influence of confinement (reduced dimensionality, size effects, quantum discreteness of elementary excitation spectra) on the superconducting state has been recognized and investigated since the 1960s. It became evident already then that thin-film and granular materials could exhibit higher critical temperatures than their bulk counterparts; subsequently, these families of low-dimensional systems were joined by nanowires and individual quantum dots. It is impractical to list even a fraction not only of the relevant papers but of the reviews that have appeared over the years. A few recent publications where additional references can be found include [1–5].

Superconductivity is also found in materials incorporating nanoparticle-sized units, for example, gallium clusters [6] and other endohedral-cluster compounds [7], arrays of colloidal nanocrystals [8, 9], and of course the doped superconducting fullerides [10].

Further development of nanoscale-based materials will benefit from the use of building blocks whose size, composition, and physical properties can be customized and accurately tuned. This is the promise of the technique known as cluster-beam deposition, see, e.g., the recent reviews [11, 12]. Specialized sources [13] are used to produce beams of metallic nanocluster particles of desired composition, which are then size-filtered by a mass spectrometer and deposited on the chosen substrate or device.[1] By varying the source parameters and nucleation conditions, it is possible to produce homogeneous, alloyed, or core–shell type nanoparticles and, in some cases, even control the particle shape [14]. The center of the size distribution can be adjusted from just several atoms per particle to hundreds or thousands, and up into the ~ 10 nm range. After undergoing size selection, the nanoparticles may be decelerated for soft-landing, so that the surface impact energy per atom is below the fragmentation limit, or, alternatively, accelerated for implantation. As distinct from colloidal nanoclusters [15], the particles are ligand-free which eliminates a need for post-processing and chemical characterization.

✉ Vitaly V. Kresin
kresin@usc.edu

[1] Department of Physics and Astronomy, University of Southern California, Los Angeles, CA 90089-0484, USA

[2] Mork Family Department of Chemical Engineering and Materials Science, University of Southern California, Los Angeles, CA 90089-1211, USA

[1] The particles are produced as ions or ionized in flight prior to size selection.

Published online: 19 October 2021

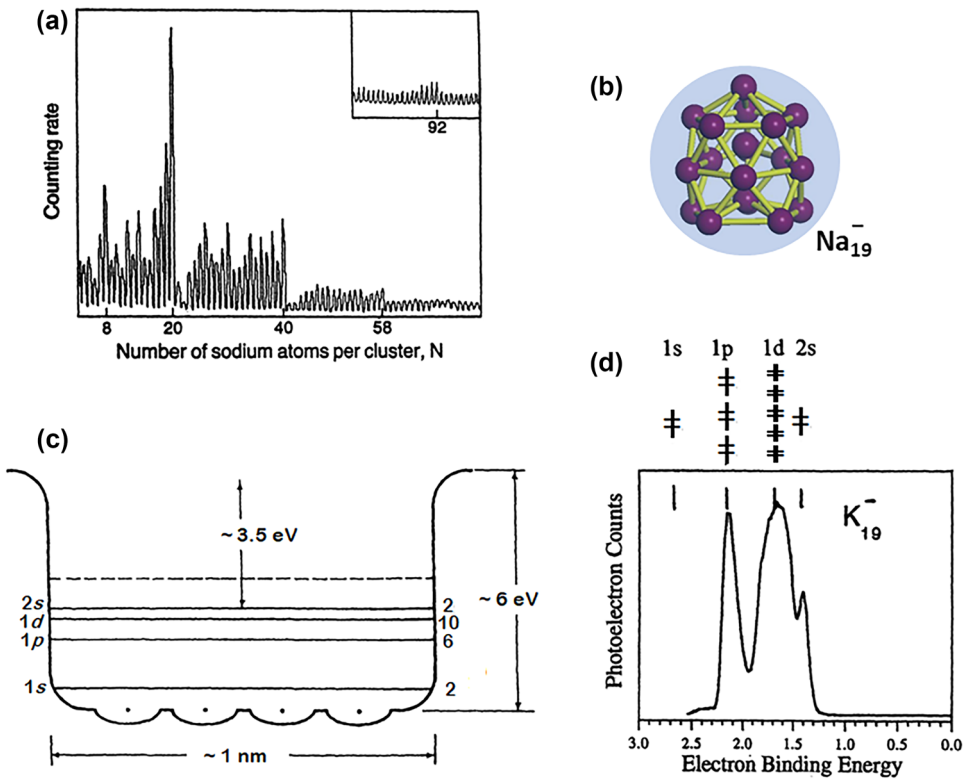

Fig. 1 Shell structure in nanoclusters of simple metals. **a** An abundance mass spectrum for Na clusters. The prominent steps are associated with electronic shells [16]. **b** The self-consistent potential which confines the delocalized electrons to the cluster is smooth, with the ionic cores screened (ionic structure of Na_{19} taken from [19]). **c** Closed-shell clusters are close to spherical and their electronic wave functions have an atomic-like shape. In this example [18], the filled shells, indicated by solid horizontal lines, accommodate 20 valence electrons. The shell label *nl* includes a radial and an angular momentum quantum number (note that there is no $l<n$ restriction for this potential well shape). **d** Photoelectron spectrum of a closed-shell potassium cluster anion with 20 valence electrons, directly showing the existence of electronic shell levels [20]. The labels and electron occupations for individual shell orbitals are shown at the top and can be compared with diagram **c**

Clearly, these techniques hold promise for research on size effects in superconductivity as well. For example, they can make it possible to optimize material composition and stoichiometry, to eliminate significant size inhomogeneities in granular compounds, to produce uniform thin films, or to fabricate current-carrying networks. The pursuit of "intelligent design" along this route requires progress in two key areas. The first is to understand superconductivity-related behavior of individual nanocluster particles, and the second is to develop schemes and devices enabling the particles to assemble without losing their distinctive useful attributes.

In Sect. 2 of this paper, we review an experiment which furnished evidence for a novel high-temperature pairing transition in free nanoclusters with size-quantized electronic states. In Sect. 3, we outline steps toward the development of prototype devices suitable for detecting superconducting transport in assemblies of size-selected nanoparticles.

2 High-T_c Pairing in "Superatom" Nanocluster Particles

A remarkable quantum size effect in nanoscience is the electronic shell structure displayed by free clusters composed of tens to thousands of atoms [16–18]. It is found in nanoclusters of many simple-metal materials. When confined to a finite particle volume, their nascent but already delocalized conduction electrons organize into discrete energy levels with clear shell ordering, akin to that in atoms or nuclei. As in the latter, the electronic states in nanoclusters are characterized by their angular momentum quantum number *l*; see Fig. 1.[2] Such nanoclusters are sometimes referred to as "superatoms" [22].

[2] More precisely, clusters with fully filled electronic shells (so-called magic numbers, named by analogy with nuclear physics) are spherical and *l* is a good quantum number. Clusters with partially filled shells find it energetically favorable to undergo a Jahn–Teller distortion into a spheroidal shape [21], in which case the electronic states can still be characterized by the angular momentum projection *m*.

The high orbital degeneracy $2(2l+1)$, which is a consequence of the quantum shell structure, leads to remarkable implications for pairing. As is known, the coupling constant λ is proportional to the electronic density of states (DOS). In a nanocluster, the DOS of the delocalized electrons is split into narrow shell levels. The resulting high degeneracy of the highest-occupied shell can qualitatively be viewed as a sharp peak in the DOS near the Fermi level, akin to a Van Hove singularity. The resulting strengthening of λ can produce a major enhancement of the gap parameter and the critical temperature. Note that in distinction to actual atoms, "superatoms" possess both a set of degenerate shell orbitals and a bath of phonons (i.e., cluster vibrations) which can provide the coupling mechanism.

It is of course meaningless to relate superconductivity in a finite Fermi system to the flow of macroscopic current. The formation of Cooper pairs of fermions (with opposite projections of orbital and spin angular momenta) is here manifested via its effect on the energy spectrum of the system. This is well known in nuclear physics and in the studies of ultracold trapped atomic gases [23, 24].

This picture led to a prediction [5, 25, 26] that in some (not all) cluster sizes, a propitious combination of a large λ and an appropriate intershell spacing can create a situation favorable for very high T_c. The work [25] was followed by publications from other theoretical groups [27–30] which supported its conclusion.

An experiment in our group confirmed this prediction [31, 32]. It was performed on a beam of nanoclusters of aluminum, which was chosen because it is a bulk superconductor and because it exhibits shell structure in cluster form. For example, the Al_{66} cluster with 198 valence electrons, which is one of those discovered to exhibit pairing, fits 30 electrons into its narrow $1j$ highest occupied shell.

As described in [31–33], the nanoclusters were produced by a sputtering/condensation source [13] (see also Fig. 4) equipped with a newly developed thermalization tube which made it possible to adjust the cluster temperature from 65 K up to several hundred K with high accuracy.

Since the clusters were studied in-flight within a molecular beam, the anticipated pairing transition was monitored by means of laser spectroscopy, namely photoelectron yield spectroscopy. The principle of the measurement is outlined in Fig. 2a, while Fig. 2b illustrates the conceptual similarity between this spectroscopic determination of the electronic DOS of the highest occupied shell and the use of tunneling spectroscopy to determine the DOS of a bulk sample.

Figure 3a shows the data obtained for the aforementioned Al_{66} nanocluster. As the temperature is lowered, a significant feature develops close to the ionization threshold. The corresponding derivative of the yield curves reveals a growing peak in the electronic DOS, as shown in Fig. 3b. Figure 3c, which plots the amplitude of the derivative maximum, reveals an electronic transition with $T_c \gtrsim 100$ K. This value exceeds the critical temperature of bulk Al by a remarkable two orders of magnitude and confirms the theoretical predictions for pairing in size-quantized clusters.

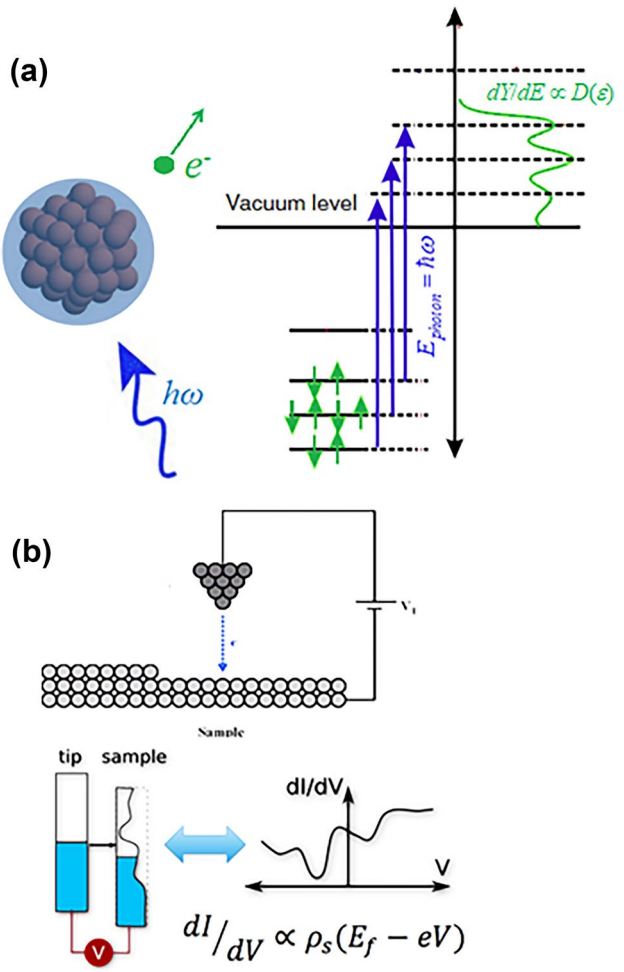

Fig. 2 **a** Mapping of the density of states of size-selected free nanoclusters. A beam of neutral clusters thermalized to a chosen temperature is ionized by a pulsed tunable laser. Cluster ions are extracted into a time-of-flight mass spectrometer, and the ion yield Y (equivalent to the photoelectron yield) is measured as a function of the photon energy E. As illustrated in the schematic diagram, $Y(E) \propto \int_{-E}^{\infty} M(\varepsilon)\rho_t(E+\varepsilon)f(\varepsilon)D(\varepsilon)d\varepsilon$ where ε is the electron energy, M the matrix element for dipole transitions from a shell level into the continuum, ρ_t the ejected electron's translational DOS, f the Fermi–Dirac function, and D the electronic DOS within the nanocluster. Since all factors but the last one are smooth functions of energy, $dY/dE \propto D(\varepsilon)$. b Photoemission can be considered an analog to tunneling spectroscopy, where the tunneling current I is given by the convolution of the sample and tip densities of states and the transmission matrix element. Therefore, the differential conductance is approximately given by $dI/dV \propto D_S(E_F\text{-}eV)$ where D_S is the sample DOS and E_F is the Fermi energy.

Indeed, a change in DOS is a well-known signature of the pairing transition. In the superconducting state, the energy

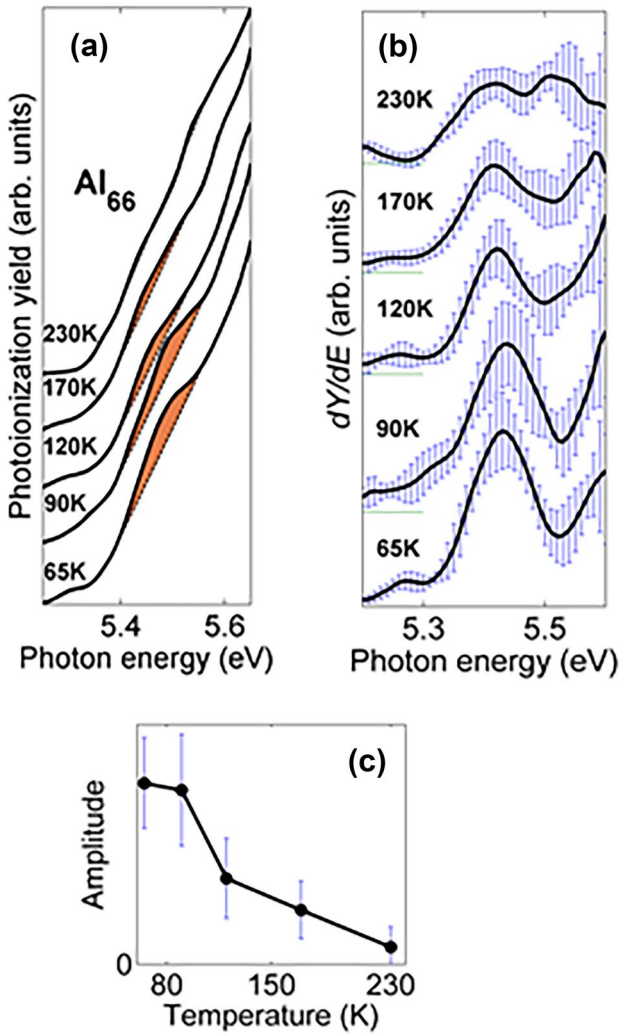

Fig. 3 **a** Photoionization yield $Y(E)$ plot for Al_{66} showing a build-up in the near-threshold electronic DOS appearing with a decrease in temperature. Only certain specific cluster sizes show such a feature. The build-up is also seen in the plots of dY/dE in panel **b**. **c** A plot of the intensity of this peak shows a transition occurring near 100 K. (The gradual decrease above the transition is assigned to pairing fluctuations expected in a finite system.) Data from [31, 32].

spectrum becomes $\xi' = (\xi^2 + \Delta^2)^{1/2}$, where ξ is the electron energy in the normal state referred to the chemical potential. In the bulk limit, this translates into a DOS of the form $D_S = D_0 \cdot \xi' / (\xi'^2 - \Delta^2)^{1/2}$, where D_0 is the DOS at the Fermi level in the normal state. In the finite cluster case, where the topmost electrons occupy a discrete shell lying below the vacuum level, the effect of pairing is to compress the highest-occupied electron shell and push it downward toward the nearby lower shells. The consequence is a peak whose intensity grows with decreasing temperature, as observed.

As discussed in [32], the characteristics of the observed transition are consistent with the theoretical predictions based on nanocluster parameters. They also do not conflict with the so-called "Anderson criterion" [34] for the observability of pairing correlations in finite systems.

A transition in the same temperature range has been detected for several other nanoclusters: Al_{37}, Al_{44}, and Al_{68}. As mentioned above, pairing in finite clusters does not occur for all sizes but only for select ones which possess an appropriate combination of shell degeneracy and inter-shell spacing. On the other hand, it is expected that such an effect also will occur in nanoclusters of other metals and in mixed (alloyed) clusters, and it is perfectly realistic for it to achieve a transition temperature reaching and exceeding room temperature.[3]

3 Prototype Geometries for Networks of Size-Selected Superconducting Nanoclusters

As described in the preceding section, quantum-sized metal nanocluster particles represent a new family of high-temperature superconductors. Given the evidence of pairing in individual nanoclusters, there exists a clear motivation to take advantage of this effect by pursuing high-temperature superconducting networks fabricated by means of carefully depositing size-resolved particles on a surface. Furthermore, it has been predicted that such systems can support a flow of lossless Josephson current orders of magnitude stronger than in conventional systems [36].

A number of reports of superconducting films assembled by size-selective cluster beam deposition have appeared in the literature; see, e.g., [37–40]. An interesting next step is to apply this technique to producing samples where superconducting nanoclusters are arranged in chains or networks, in sufficient quantity to affect the transport properties but sufficiently separated to preserve their individuality. This remains a work in progress; in this section, we illustrate some prototype deposition geometries under development in our laboratory.

The cluster deposition setup is outlined in Fig. 4. It produces pure (ligand-free) size-selected metal or alloy nanoparticles by sputtering atomic vapor from a metallic target,

[3] A natural question arises whether an experiment of this type can detect the effect of a magnetic field, such as the Meissner effect or the disruption of pairing. Unfortunately, this appears very difficult at present. The penetration depth exceeds the nanocluster diameter, making flux expulsion unobservable. As for the critical field, its estimated magnitude for high-T_c nanoparticles is so high, ~ 10 T, that coupling such a magnet to a molecular beam apparatus (and not disrupting the operation of its mass spectrometer) is technically extremely challenging. Possibly, spectroscopy of cold cluster anions in a Penning cluster trap [35] could provide such a means, but such traps normally operate at a fixed value of the magnetic field. Therefore, magnetic field measurements may require samples of deposited size-selected nanoclusters; see the next section.

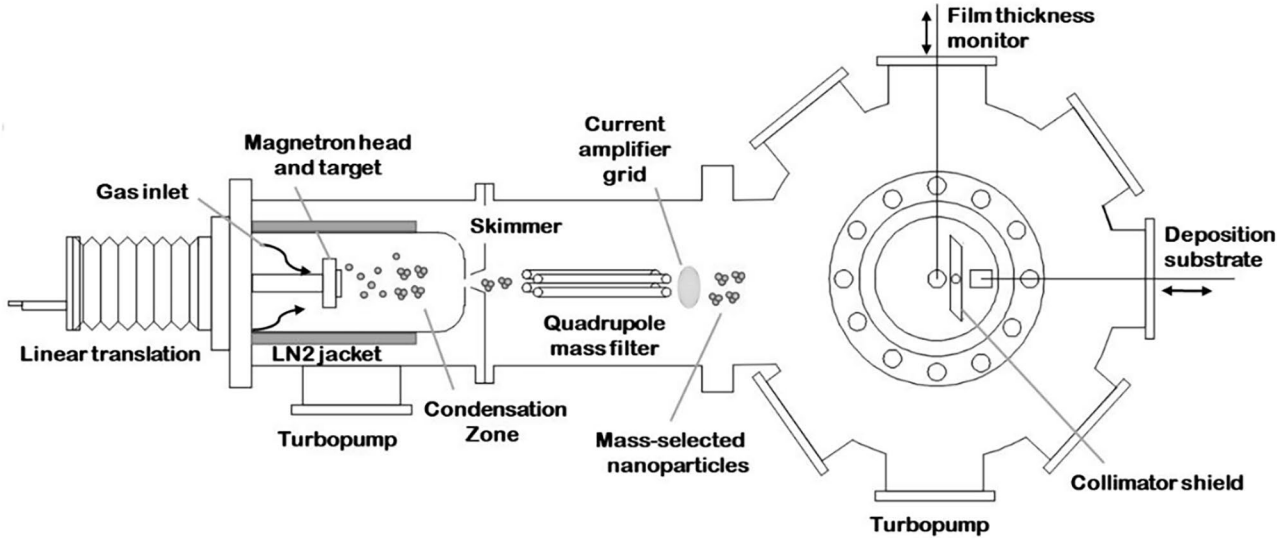

Fig. 4 The nanoparticle deposition system uses a magnetron gas aggregation source and a quadrupole mass filter manufactured by Mantis Deposition Ltd. (succeeded by Nikalyte Ltd.). Sputtered metal atoms and ions enter the liquid nitrogen-cooled condensation zone where they undergo collisions with cold argon and helium gases. Nanocluster ions form and grow as the mixture moves through the source toward the exit aperture. The ions are mass-filtered by a quadrupole equipped with an ion flux measurement grid and enter the deposition chamber. Here, they can be slowed down by a retarding potential for soft-landing on the selected substrate or device. It typically takes on the order of a few minutes to achieve near-monolayer coverage of the surface by nanoparticles

condensing it within a flow of cold gas, and generating a nanoparticle beam as the flow leaves the condensation zone via a small aperture [13]. The operation is analogous to that of the source used for experiments described in Sect. 2. This type of nanoparticle source, invented at the University of Freiburg [41], is commonly referred to as a "magnetron sputtering/aggregation" or a "terminated cluster growth" source. For prototype development, we employed silver and aluminum nanoparticles of several nm diameter.

Since nanoclusters land on the surface randomly, producing an organized arrangement requires either manipulating them post-deposition or providing a template for them to arrange themselves on. Carbon-based surfaces such as graphene and carbon nanotubes (CNTs) are convenient choices for this purpose. For example, it was found that Ag_{561} clusters soft-landed on a C_{60} monolayer are not significantly deformed by the surface [42]. The bonding to the surface is sufficiently weak to allow nanomanipulation, and extensive research on graphene and CNT devices has established useful design, fabrication, and characterization techniques.

Furthermore, both metallic CNT and single-layered graphene devices can display proximity-induced superconductivity, as has been demonstrated by using metallic contacts in the case of CNT's and by using small islands for graphene [43–45]. Hence, such supports can respond and signal when nanoclusters in contact with them transition into the superconducting state.

A 4-point graphene channel device is shown in Fig. 5a. Twenty-five field-effect transistors were fabricated in parallel by electron-beam lithography on a 1 cm^2 die of CVD-grown graphene on a Si/SiO_2 substrate (Grolltex, Inc.). The procedure, as well as the protocols for removing the PMMA resin residue and for the bakeout of the graphene and the substrate, is described in detail in [46]. Figure 5b shows the channel after size-selective nanoparticle deposition. Conveniently, we found that due to the difference in surface attractive forces, the particles almost exclusively coat the graphene and not the surrounding SiO_2. The samples can be mounted into chip carrier sockets and subsequently probed either in situ or in an external transport measurement system.

With such an arrangement, one can already in principle search for the appearance of the proximity effect in the graphene channel due to nanocluster superconductivity. In addition, by gating the device, one can adjust the carrier level within its graphene layer, modifying its mobility as well as inducing charge transfer into the deposited nanoparticles.

For the purposes of constructing a tunneling network or chain of nanoparticles, they need to be arranged into a regular array post-deposition. With the help of an atomic force microscope (AFM) tip, the nanoparticles can be manipulated into chains or other formations on the graphene substrate, as illustrated in Fig. 5c.

Another approach to generating an ordered chain of nanoclusters is to deposit them onto a suspended metallic

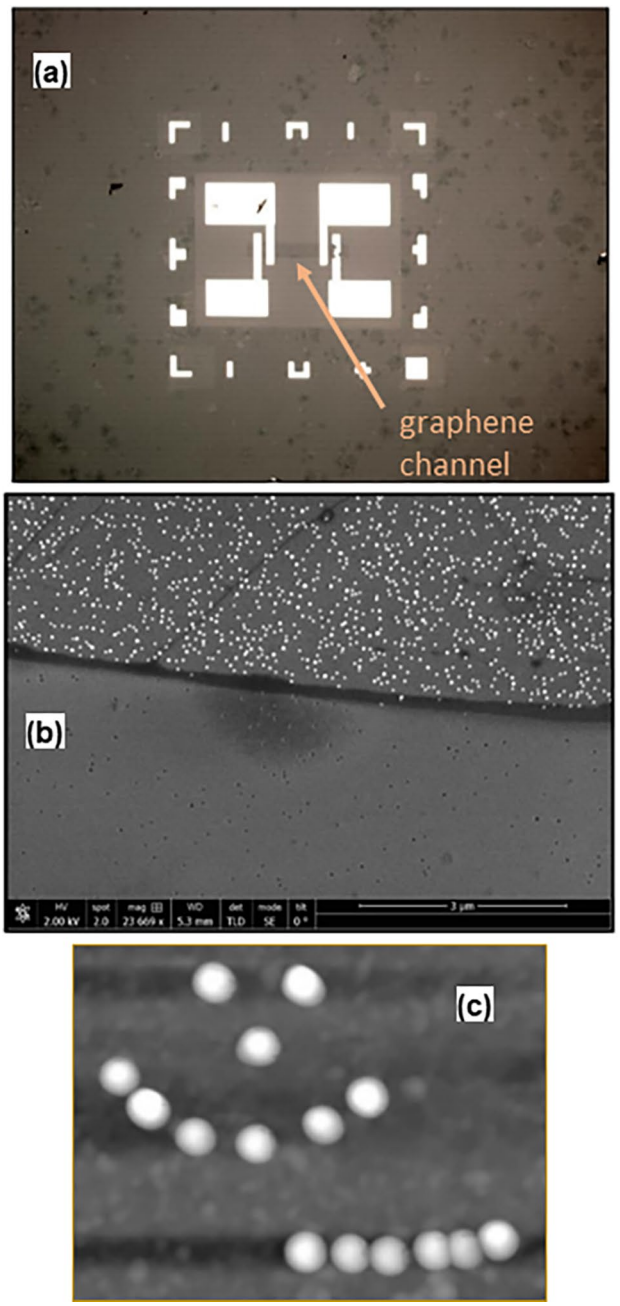

Fig. 5 **a** An optical microscopy image of a four-terminal device for the measurement of conductivity across a graphene channel. Its back gate allows for the graphene carrier concentration to be varied. **b** A scanning electron microscope image of 10 nm Ag nanoparticles soft-landed on the graphene channel in this device. The coverage density can be adjusted over a wide range. **c** AFM nanomanipulation of deposited Ag nanoparticles into arrays and other formations on the graphene surface.

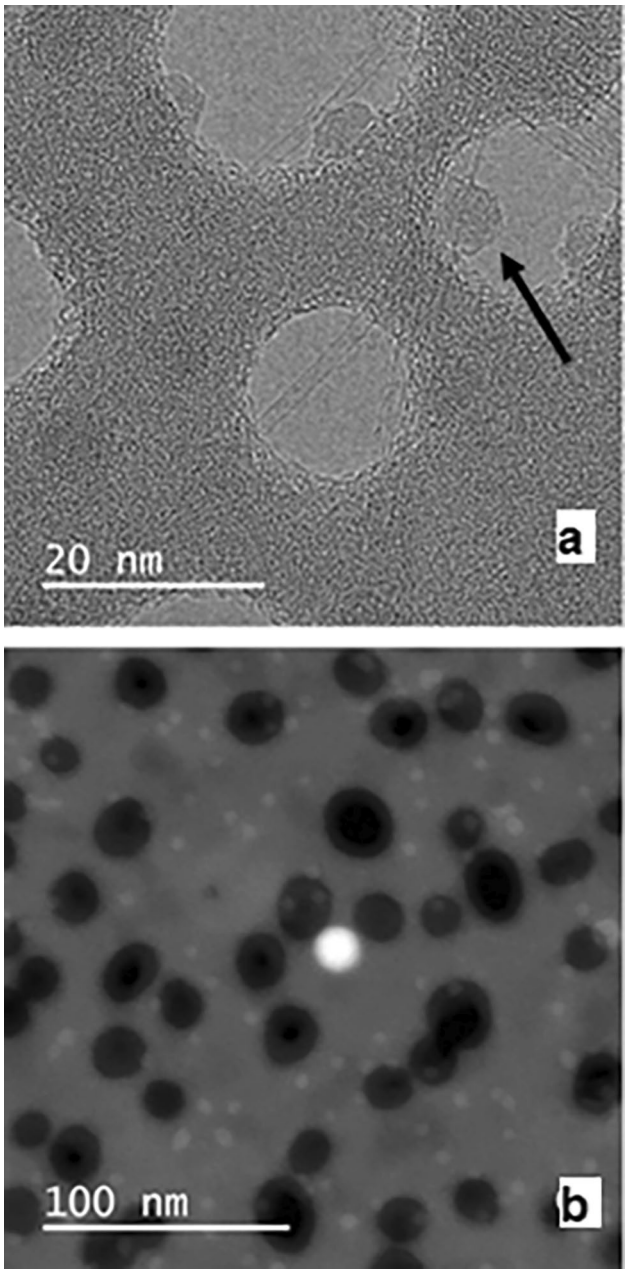

Fig. 6 TEM images of Al nanoparticles landed on single-walled CNTs on a nanoporous SiN TEM grid [48]. **a** A deposited aluminum nanocluster (arrow) on a suspended CNT. **b** A lower-magnification annular dark field scanning TEM image shows nanoparticles (gray) suspended over the grid's nanopores (dark). (The bright spot is an artifact due to the electron beam.)

CNT. With sufficient deposition density, this "beads-on-a-string" arrangement will produce a one-dimensional tunneling nanoparticle array. At lower coverage, the transition of individual nanoclusters into the superconducting state will manifest itself as a change in nanotube conductance, either via the proximity effect, as mentioned above, or via nanoclusters acting as shunts.

Decoration of suspended CNTs by ligand-free metal particles was originally performed by atomic vapor deposition [47]. The metal atoms subsequently coalesced into nanoparticle islands. Recently, we demonstrated [48] that

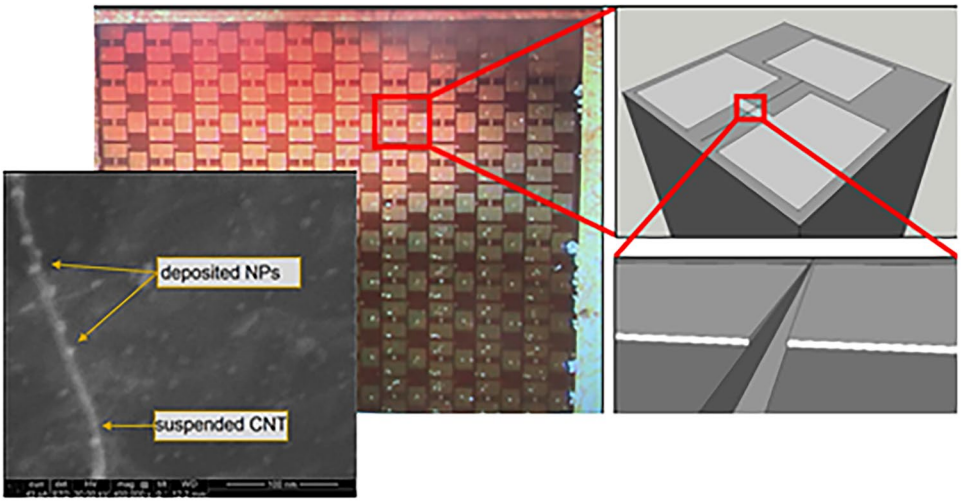

Fig. 7 Inset on bottom left: a carbon nanotube suspended over a trench and subjected to deposition of 5 nm silver nanoparticles, forming a chain. Center: an optical microscopy image of a 0.5 cm by 0.5 cm array of microtrenches. Right: design model of one 3-electrode microtrench device and a zoomed-in image of the trench area

it is possible to deposit size-selected nanoparticles from a beam onto neat unbundled single-walled CNTs dropcast onto nanoporous grids and image them by transmission electron microscopy (TEM) (Fig. 6).

A further development is a nanotube field-effect transistor based on CNTs grown over trenches etched in a Si/SiO_2/Si_3N_4 substrate by catalyst-enabled chemical vapor deposition. The design and fabrication of such devices are described in [46, 49]. As with the graphene devices described above, a die containing multiple functioning transistors is fabricated and placed into ceramic chip packages or AFM sample pucks. A representative device and an image of a CNT decorated with deposited metal nanoparticles are shown in Fig. 7. This design is well-suited for the studies of temperature-dependent transport and the detection of a superconducting transition.

4 Summary

Size-selected metal nanoclusters with electronic shell structure establish a new class of high-temperature superconductors, which may be extended to still much higher critical temperatures by the optimization of material, size, and composition. They offer a platform for interesting novel physical studies and represent promising building blocks for high-Tc materials, devices, and networks. The latter direction can be achieved with the help of size-selective soft-landing of nanoclusters, in combination with the development of surface templates and nanomanipulation methods.

Acknowledgements We would like to thank Dr. A. Bushmaker and Dr. S. Stuart (Aerospace Corp.), and Prof. M. El-Naggar, Prof. S. Cronin, M. Chavez, C. Cole, and J. Farmer (USC) for valuable advice, collaboration, and access to and help with technical facilities related to recent work described in Section 3.

Funding This research was supported by the U.S. National Science Foundation under Grant No. DMR-2003469.

References

1. Von Delft, J., Ralph, D.C.: Spectroscopy of discrete energy levels in ultrasmall metallic grains. Phys. Rep. **345**, 61–173 (2001)
2. Peeters, F.M., Shanenko, A.A., Croitoru, M.D.: Nanoscale superconductivity. In: Sattler, K. D. (ed.) Handbook of Nanophysics. **1**. CRC Press, Boca Raton (2010)
3. Bose, S., Ayyubon, P.: A review of finite size effects in quasi-zero dimensional superconductors. Rep. Prog. Phys. **77**, 116503 (2014)
4. Valentinis, D., Berthod, C.: Periodicity of superconducting shape resonances in thin films. Phys. Rev. B. **102**, 054518 (2020)
5. Kresin, V.Z., Ovchinnikov, S.G., Wolf, S.A.: Superconducting state: mechanisms and materials, Sec. 6.5. Oxford University Press, Oxford (2021)
6. Bakharev, O.N., Bono, D., Brom, H.B., Schnepf, A., Schnöckel, H., de Jongh, L.J.: Superconductivity in a molecular metal cluster compound. Phys. Rev. Lett. **96**, 117002 (2006)
7. Verchenko, V.Y., Shevelkov, A.V.: Endohedral cluster intermetallic superconductors: at the frontier between chemistry and physics. Dalton Trans. **50**, 5109–5114 (2021)
8. Weitz, I.S., Sample, J.L., Ries, R., Spain, E.M., Heath, J.R.: Josephson coupled quantum dot artificial solids. J. Phys. Chem. B **104**, 4288–4291 (2000)
9. Zolotavin, P., Guyot-Sionnest, P.: Superconductivity in films of Pb/PbSe core/shell nanocrystals. ACS Nano **6**, 8094–8104 (2012)
10. Gunnarsson, O.: Alkali-doped fullerides. World, Singapore (2004)
11. Popok, V.N., Kylián, O.: Gas-phase synthesis of functional nanomaterials. Appl. Nano **1**, 25–58 (2020)
12. Milani, P., Sowwan, M. (eds.): Cluster beam deposition of functional nanomaterials and devices. Elsevier, Amsterdam (2020)
13. Huttel, Y. (ed.): Gas-phase synthesis of nanoparticles. Wiley-VCH, Weinheim (2017)
14. Xia, Y., Nelli, D., Ferrando, R., Yuan, J., Li, Z.Y.: Shape control of size-selected naked platinum nanocrystals. Nat. Commun. **12**, 3019 (2021)
15. Jin, R., Zeng, C., Zhou, M., Chen, Y.: Atomically precise colloidal metal nanoclusters and nanoparticles: fundamentals and opportunities. Chem. Rev. **116**, 10346–10413 (2016)

16. de Heer, W.A., Knight, W.D., Chou, M.Y., Cohen, M.L.: Electronic shell structure and metal clusters. In: Ehrenreich, H., Turnbull, D. (eds.) Solid State Phys. **40**, 93–181. Academic, New York (1987)
17. de Heer, W.A.: The physics of simple metal clusters: experimental aspects and simple models. Rev. Mod. Phys. **65**, 611–676 (1993)
18. Kresin, V.V., Knight, W.D.: Quantized electron states in metal microclusters: electronic shells, structural effects, and correlations. In: Kresin, V.Z. (ed.) Pair Correlations in Many-Fermion Systems, 245–261. Plenum, New York (1998)
19. Sun, W.G., Wang, J.J., Lu, C., Xia, X.X., Kuang, X.Y., Hermann, A.: Evolution of the structural and electronic properties of medium-sized sodium clusters: a honeycomb-like Na20 cluster. Inorg. Chem. **56**, 1241–1248 (2017)
20. Eaton, J.G., Kidder, L.H., Sarkas, H.W., McHugh, K.M., Bowen, K.H.: Photoelectron spectroscopy of alkali metal cluster anions. In: Schmidt, R., Lutz, H.O., Dreizler, R. (eds.) Nuclear Physics Concepts in the Study of Atomic Cluster Physics, 291–304. Springer, Berlin (1992)
21. Clemenger, K.: Ellipsoidal shell structure in free-electron metal clusters. Phys. Rev. B **32**, 1359–1362 (1985)
22. Khanna, S., Jena, P.: Atomic clusters: building blocks for a class of solids. Phys. Rev. B **51**, 13705–13716 (1995)
23. Broglia, R. A., Zelevinsky, V. (eds) Fifty years of nuclear BCS: pairing in finite systems. World, Singapore (2013)
24. Strinati, G.C., Pieri, P., Röpke, G., Schuck, P., Urban, M.: The BCS–BEC crossover: from ultra-cold Fermi gases to nuclear systems. Phys. Rep. **738**, 1–76 (2018)
25. Kresin, V.Z., Ovchinnikov, Y.N.: Shell structure and strengthening of superconducting pair correlation in nanoclusters. Phys. Rev. B **74**, 024514 (2006)
26. Kresin, V.Z., Ovchinnikov, Y.N., Friedel, J.: Pair correlation and dynamic Jahn-Teller effect: High Tc in nanoclusters. Europhys. Lett. **108**, 43001 (2014)
27. Kuzmenko, N.K., Mikhajlov, V.M.: Pairing in spherical nanograins. Physica. C. **470**, 193–201 (2010)
28. Baturin, V.S., Losyakov, V.V.: On heat capacity of nanoclusters with a shell structure. J. Exp. Theor. Phys. **112**, 226–231 (2011)
29. Croitoru, M.D., Shanenko, A.A., Kaun, C.C., Peeters, F.M.: Metallic nanograins: spatially nonuniform pairing induced by quantum confinement. Phys. Rev. B **83**, 214509 (2011)
30. Lindenfeld, Z., Eisenberg, E., Lifshitz, R.: Possibility of electron pairing in small metallic nanoparticles. Phys. Rev. B **84**, 064532 (2011)
31. Halder, A., Liang, A., Kresin, V.V.: A novel feature in aluminum cluster photoionization spectra and possibility of electron pairing at T≳100 K. Nano Lett. **15**, 1410–1413 (2015)
32. Halder, A., Kresin, V.V.: Spectroscopy of metal "superatom" nanoclusters and high-Tc superconducting pairing. Phys. Rev. B **92**, 214506 (2015)
33. Halder, A.: Temperature-dependent photoionization and electron pairing in metal nanoclusters. PhD dissertation, University of Southern California, Los Angeles (2015)
34. Anderson, P.W.: Theory of dirty superconductors. J. Phys. Chem. Solids **11**, 26–30 (1959)
35. König, S., Jankowski, A., Marx, G., Schweikhard, L., Wolfram, M.: Fission of polyanionic metal clusters. Phys. Rev. Lett. **120**, 163001 (2018)
36. Ovchinnikov, Y.N., Kresin, V.Z.: Cluster-based superconducting tunneling networks. Phys. Rev. B **85**, 064518 (2012)
37. Riefer, G., Höcketstailer, M., Jerger, T.H., Nassal, B., Pflaum, R., Recknagel, E.: Superconducting lead cluster films with particle size dependent reduction of Tc. Z. Phys. D **20**, 337–339 (1991)
38. Vossloh, C., Holdenried, M., Micklitz, H.: Influence of cluster size on the normal- and superconducting-state properties of granular Bi films. Phys. Rev. B **58**(12), 422–12426 (1998)
39. Cuppens, J., Romero, C.P., Lievens, P., Van Bael, M.J.: Superconductivity in Pb cluster assembled systems with different degrees of coagulation. Phys. Rev. B **81**, 064517 (2010)
40. Houben, K., Jochum, J.K., Couet, S., Menéndez, E., Picot, T., Hu, M.Y., Zhao, J.Y., Alp, E.E., Vantomme, A., Temst, K., Van Bael, M.J.: The influence of phonon softening on the superconducting critical temperature of Sn nanostructures. Sci. Rep. **10**, 5729 (2020)
41. Haberland, H., Mall, M., Moseler, M., Qiang, Y., Reiners, T., Thurner, Y.: Filling of micron-sized contact holes with copper by energetic cluster impact. J. Vac. Sci. Technol. A **12**, 2925–2930 (1994)
42. Duffe, S., Irawan, T., Bieletzki, M., Richter, T., Sieben, B., Yin, C., von Issendorff, B., Moseler, M., Hövel, H.: Softlanding and STM imaging of Ag561 clusters on a C60 monolayer. Eur. Phys. J. D **45**, 401–408 (2007)
43. Kasumov, A., Kociak, M., Ferrier, M., Deblock, R., Guéron, S., Reulet, B., Khodos, I., Stéphan, O., Bouchiat, H.: Quantum transport through carbon nanotubes: proximity-induced and intrinsic superconductivity. Phys. Rev. B **68**, 214521 (2003)
44. Feigel'man, M.V., Skvortsov, M.A., Tikhonov, K.S.: Theory of proximity-induced superconductivity in graphene. Solid State Commun. **149**, 1101–1105 (2009)
45. Han, Z. Allain, A., Arjmandi-Tash, H., Tikhonov, K., Feigel'man, M., Sacépé, B., Bouchiat, V.: Collapse of superconductivity in a hybrid tin-graphene Josephson junction array. Nat. Phys. **10**, 380–386 (2014)
46. Edwards, P. J.: The adsorption and selective deposition of molecular and nanocluster ions on carbon based devices. PhD dissertation, University of Southern California, Los Angeles (2021)
47. Zhang, Y., Franklin, N.W., Chen, R.J., Dai, H.: Metal coating on suspended carbon nanotubes and its implication to metal–tube interaction. Chem. Phys. Lett. **331**, 35–41 (2000)
48. Khojasteh, M., Mecklenburg, M. H., Edwards, P. J., Lefebvre, J., Ding, J., Malenfant, P. R., Kresin, V. V.: Decoration of suspended single-walled carbon nanotubes with soft-landed size-selected metal nanoparticles. Thin Solid Films. **699**, 137907 (2020)
49. Bushmaker, A.W., Deshpande, V.V., Bockrath, M.W., Cronin, S.B.: Direct observation of mode selective electron−phonon coupling in suspended carbon nanotubes. Nano Lett. **7**, 3618–3622 (2007)